Dynamics of antiferroelectric phase transition in PbZrO_{3}

Z. G. Fthenakis and I. Ponomareva

Phys. Rev. B **96**, 184110 — Published 27 November 2017

DOI: 10.1103/PhysRevB.96.184110

Dynamics of antiferroelectric phase transition in $PbZrO_3$

Z. G. Fthenakis[1] and I. Ponomareva[1]

[1] *Department of Physics, University of South Florida, Tampa, Florida 33620, USA*

Abstract

The dynamics of the phase transition in antiferroelectric $PbZrO_3$ which is a subject of a decades long debate, is examined using first-principles-based simulations. This is achieved through development of a computational approach that allows calculations of generalized complex susceptibilities at an arbitrary point of the Brillouin zone. Application of this approach to the case of $PbZrO_3$ predicts the temperature evolution of many of its lattice modes, some of which remain elusive or even "invisible" in experiments. The computational data suggest that two lattice modes are primarily responsible for the antiferroelectric phase transition in this material: the one associated with oxygen octahedra tilts dynamics and the other due to lead ions antipolar vibrations.

PACS numbers: 77.22.-d, 77.84.-s, 77.22.Ch, 78.30.-j, 77.80.-e, 77.80.B-

I. INTRODUCTION

Antiferroelectric (AFE) $PbZrO_3$ has recently become a subject for an intense reinvestigation owing to its status of a prototypical antiferroelectric[1–3]. It undergoes a single phase transition from paraelectric cubic to AFE *Pbam* phase around 505 K[1]. Such transition is associated with a condensation of two order parameters described by the wave vectors $\mathbf{q}_{\Sigma_2} = \frac{2\pi}{a}(1/4, 1/4, 0)$ (antiparallel shifts of the lead ions) and $\mathbf{q}_{R_4^+} = \frac{2\pi}{a}(1/2, 1/2, 1/2)$ (antiphase tilts of oxygen octahedra)[4], and the onset of spontaneous strain[5]. In addition, there exists a large increase in static dielectric susceptibility on approaching the phase transition. Interestingly, such a large increase is not necessary for antiferroelectricity, according to the first model of antiferroelectrics[6]. At the same time, what is required for antiferroelectricity is the existence of a ferroelectric (FE) phase that is energetically competitive with the AFE one[7]. This feature allows to stabilize FE phase by an application of an electric field and is responsible for a typical double loop structure of the electric hysteresis loops in antiferroelectrics. The structural distortions associated with the phase transition in $PbZrO_3$ include R_4^+, Σ_2, S_4, R_5^+, X_3^-, and M_5^- distortions listed in the order of their decreasing contribution to the energy gain due to a transition[8]. To elucidate the fundamental origin of a phase transition one usually turns to the soft mode theory of phase transitions, which relates phase transition to the critical slowing down (softening) of one of the lattice modes[7]. Within mean-field theory it can be shown that a critical slowing down of zone center transverse optical mode gives rise to the large increase (or theoretically, divergence) of the static dielectric susceptibility[7]. To establish the presence of soft mode(s) a detailed investigation of the temperature evolution of modes dynamics is necessary. The modes that exhibit strongest temperature anomalies are assumed to be primarily responsible for the phase transition. While this approach works really well for the case of ferroelectrics, whose instability is associated with softening of infrared (or in some cases Raman active) zone center modes, antiferroelectrics, whose instability is associated with off-center mode(s), turn out to be far more difficult to study. $PbZrO_3$ is one of such examples. As a result the origin of the phase transition in these materials has remained debatable for decades[9–12]. Originally it was proposed that two modes (zone center and off-center ones) should exhibit softening[9] which was consistent with indirect experimental evidence[10]. Later however, a study on $PbZrO_3$ ceramics[11] revealed only slight softening of the zone-center modes and assigned strong di-

electric anomaly at the Curie point to the central mode. Very recently, a combination of experimental and theoretical tools led to the proposal of a new mechanism for the AFE phase transition that includes softening of a single lattice mode (the ferroelectric soft mode in perovskites) that gives rise to the AFE phase transition with the help of the flexoelectric coupling[2]. To add to the controversy of the subject, another recent study used a combination of experimental techniques to propose that $PbZrO_3$ exhibits a flat soft polarization branch which, however, does not have a local minimum near the AFE wave vector[3]. In this model, the stabilization of the AFE phase requires coupling to oxygen octahedra tilt mode via a trilinear term, which is consistent with the first-principles findings of Ref.13. While these models clarify certain aspects of the phase transition in $PbZrO_3$, they aim at explaining a certain set of experimental data, which, despite the recent progress in measurements, still remains limited, owing to the fundamental difficulties in tracing temperature evolution of modes in this material. This raises one interesting question: can we use first-principles-based simulations to overcome these fundamental difficulties and provide atomistic insight to the nature of the AFE phase transition in $PbZrO_3$?

The aims of this paper are: i) to propose a first-principles-based approach suitable to study mode dynamics at an arbitrary point of the Brillouin zone and at finite temperatures; ii) to predict temperature evolution of modes responsible for the AFE phase transition in $PbZrO_3$ in a wide temperature range; and iii) to provide first-principles-based insight into the nature of the AFE phase transition in $PbZrO_3$.

II. THE METHOD

To achieve our methodological goal we developed Molecular Dynamics (MD) for the effective Hamiltonian proposed in Ref.8. The degrees of freedom for the effective Hamiltonian include polar local modes, $\mathbf{u}_i$, which are proportional to the local dipole moment in the unit cell i and describe the AFE instability at Σ_2 point of the Brillouin zone, antiferrodistortive (AFD) local modes, $\mathbf{w}_i$, that describe oxygen octahedra tilts about Cartesian axes and are responsible for the R_4 point instability, and inhomogeneous and homogeneous strain variables, which describe elastic deformations of the unit cell and supercell, respectively. The Hamiltonian includes energy associated with the antiferroelectric Σ_2 mode and contains contributions from the dipole-dipole interactions, short-range interaction, and on-site self-

energy. It also includes energy due to the AFD mode that is similar to the previous one but excludes the dipole-dipole interactions as AFD local modes are nonpolar. Finally, the Hamiltonian includes the energy associated with elastic deformations. All degrees of freedom are coupled with each other by the symmetry allowed interactions. All parameters of the effective Hamiltonian are derived from the local-density-approximation-based density functional theory calculations[8]. This Hamiltonian correctly reproduces the sequence of phase transition in $PbZrO_3$, its electrical properties and behavior under pressure[8].

In MD the Hamiltonian is used to compute forces acting on all the degrees of freedom (9 per unit cell of the cubic perovskite structure plus six homogeneous strain variables for the entire supercell). The Newton equations of motion are then set up and numerically integrated for all degrees of freedom with the integration step of 1 fs. The following masses are used for the polar local mode, AFD local mode, and inhomogeneous strain variables: 54.3, 16.0 and 346.4 au, respectively. For the homogeneous strain mass we used the value of 148,936 au. Bulk $PbZrO_3$ is simulated with the supercell of 16x16x16 unit cells of cubic perovskite with periodic boundary conditions applied along all three Cartesian directions. First we obtain equalibrated supercells in the temperature range of 0 to 2000 K by using the simulated annealing approach. In such an approach the simulations begin at 2000 K and the supercell is slowly annealed down to the temperature of 5 K in steps of 5 K. Smaller temperatures steps of 1 K were used in the vicinity of the phase transition. For each temperature we simulate 50,000 MD steps of NPT ensemble (constant number of particles, pressure, and temperature). Pressure is set to zero, while the temperature control is achieved via the Evans-Hoover thermostat[14].

III. RESULTS AND DISCUSSION

Fig.1 shows the temperature evolution of the AFE and AFD order parameters as well as $1 - c/a$ ratio, where a and c are the two lattice constants of orthorhombic $PbZrO_3$. The phase transition occurs at 944 K (which overestimates the experimental value of 505 K) and is associated with the simultaneous onset of AFE, AFD and strain order parameters. This result is in agreement with the Monte Carlo simulations reported in Ref.8.

Next, we use the equilibrated supercells to investigate the dynamics of the modes that originate from the dynamics of the local polar modes and AFD oxygen octahedra tilts.

Technically, in these simulations the shape and volume of the supercell is fixed at their equilibrium values to allow for accurate simulations of the modes dynamics. To access mode dynamics at an arbitrary point of the Brillouin zone we use the concept of generalized complex susceptibility, $\chi(\mathbf{q},\nu)$, which describes the response of the system to a staggered time dependent generalized field, $\mathbf{X}(\mathbf{q},t)$, with the wave vector $\mathbf{q}$. The response of the system is quantified by a generalized polarization, $\mathbf{x}(\mathbf{q},t)/V$, where $\mathbf{x}(\mathbf{q},t)$ is the generalized total dipole moment of the wave with the wave vector $\mathbf{q}$ and V is the supercell volume. For example, the generalized polarization due to electric dipoles wave with $\mathbf{q}_{\Sigma_2}$ gives the AFE order parameter (or antipolar vector) in $PbZrO_3$, while the generalized polarization due to AFD oxygen octahedra tilts wave with $\mathbf{q}_{R_4^+}$ gives the AFD order parameter. Generalized polarization for $\mathbf{q}_{\Sigma_2}$ also describe the response of the system to a staggered electric field, while generalized polarization for $\mathbf{q}_{R_4^+}$ describes the response of the system to a hypothetical staggered field capable of exciting oxygen octahedra tilts mode. Of course, in the trivial case of $\mathbf{q}_\Gamma = (0,0,0)$ the generalized polarization reduces to the electric polarization, while the generalized field becomes homogeneous electric field. The interaction of the system with the generalized fields contributes $-\mathbf{x}(\mathbf{q},t)\cdot\mathbf{X}(\mathbf{q},t)$ to the Hamiltonian. While not all of generalized susceptibilities could be measured experimentally, they provide a valuable insight into the mode dynamics available only from computations. The extension of the linear response theory[15,16] to this case yields the following expression for the generalized susceptibility

$$\begin{aligned}\chi_{\alpha\beta}(\mathbf{q},\nu) = \frac{1}{\varepsilon_0 V k_B T}\Bigg\{ &\langle x_\alpha(\mathbf{q}) x_\beta(\mathbf{q})\rangle - \langle x_\alpha(\mathbf{q})\rangle\langle x_\beta(\mathbf{q})\rangle \\ &+ i2\pi\nu\int_0^\infty dt e^{i2\pi\nu t}\langle (x_\alpha(\mathbf{q},t=0) - \bar{x}_\alpha(\mathbf{q},t=0))(x_\beta(\mathbf{q},t) - \bar{x}_\beta(\mathbf{q},t))\rangle\Bigg\}.\end{aligned} \tag{1}$$

Here $x_\alpha(\mathbf{q})$ is the α Cartesian component of the total generalized dipole moment with the wavevector $\mathbf{q}$ computed as $\mathbf{x}(\mathbf{q}) = Z^\star \sum_i \mathbf{u}_i int(e^{i\mathbf{q}\cdot\mathbf{r}})$ for the modes originating from the polar local modes, $\mathbf{u}_i$, ($Z^\star$ is the Born effective charge), and as $\mathbf{x}(\mathbf{q}) = \sum_i \mathbf{w}_i int(e^{i\mathbf{q}\cdot\mathbf{r}})$ for the modes originating from the AFD tilts, $\mathbf{w}_i$. In Eq.(1) $\mathbf{r}$ gives the position of the unit cell within the supercell and *int* indicates nearest integer value. Note, that ε_0 in the denominator is only required for the susceptibilities due to polar modes and can be omitted in all other cases. The first two terms in Eq.(1) describe the response of the system to a static field.

Both $\langle ... \rangle$ and bars indicate the ensemble average.

In the present work we are interested in the dynamics of the modes that originate from the Σ_2 antipolar distortions and R_4^+ AFD distortions. Therefore, we compute the generalized susceptibilities due to the polar local mode at Σ_2 point of the parent Brillouin zone (PBZ) of the cubic structure and due to AFD local mode at R_4^+ point of the PBZ. They are denoted as χ_{AFE} and χ_{AFD}, respectively. In addition, we also compute the complex dielectric susceptibility, χ_{FE}, which gives access to the zone center modes of the *Pbam* structure, Technically, for a given temperature the dynamics of the supercell is followed during 3 ns to collect 2500 autocorrelation functions, $(x_\alpha(\mathbf{q}, t=0) - \bar{x}_\alpha(\mathbf{q}, t=0))(x_\beta(\mathbf{q}, t) - \bar{x}_\beta(\mathbf{q}, t))$, each of 10 ps duration using the overlap technique[14]. These autocorrelation functions are first averaged and then the result is Fourier transformed as indicated by Eq.(1). The real and imaginary parts of the components of susceptibility tensors are fitted with a sum of damped harmonic oscillator functions which contains up to 4 terms[17]. The fitting yields the intrinsic frequencies of the modes as fitting parameters. The amplitudes, A, for different complex generalized susceptibilities as obtained from the fit are given in Fig.2 for a representative temperature above and below the Curie point. Fig.2(a) indicates that in the paraelectric phase (1400 K) there exists a single mode that describes polar ionic vibrations, while in the AFE phase (100 K) we find four modes. One of these mode (103 cm^{-1}) is associated with polar vibrations along the nonpolar direction of AFE $PbZrO_3$, while the rest is associated with the polar ionic vibrations along the antipolar direction of AFE $PbZrO_3$. Fig.2(b) shows that there exists a single mode associated with oxygen octahedra tilts dynamics above the Curie point. Below the Curie point we find 6 modes that involve oxygen octahedra dynamics. Two of them (82 and 152 cm^{-1}) are associated with oxygen octaherda tilts about the nonpolar axis of AFE $PbZrO_3$, while the rest originates from the dynamics of the tilts about the antipolar axis. Fig.2(c) reveals three modes at Σ_2 point of the PBZ above the Curie temperature. The highest frequency mode is associated with antipolar vibrations along the direction of the wave vector, while the other two are associated with vibrations along the two directions perpendicular to the direction of the wave vector. The lowest frequency mode is the one to give origin to the AFE order parameter and especially important for the phase transition. Below the Curie point we find six modes. Half of them are associated with antipolar vibrations along the nonpolar direction of AFE $PbZrO_3$, while the rest is associated with the vibrations along the antipolar axis of the structure.

To elucidate the origin of the phase transition in $PbZrO_3$ we trace the temperature evolution of the intrinsic frequencies associated with all these modes. Fig.3 gives our computational results along with experimental data from Ref.3. Note, that in order to facilitate comparison between computational and experimental data computational temperatures are rescaled to reproduce experimental Curie point. We begin with the zone-center modes given in Fig.3(a). In the paraelectric phase the sole polar mode shows some softening on approaching the phase transition. In the AFE phase two of the modes (the one shown by red diamonds and one of the black circles) show moderate softening, while others respond very little to the temperature. As a result we expect rather moderate increase in the static dielectric constant at the Curie point[7]. Indeed, our computational data given in the inset to Fig.3 show an increase in the static dielectric constant but no divergence. This finding confirms that the divergence of the dielectric constant is not required for the AFE phase transition[6]. The temperature evolution of the modes that involve oxygen octahedra tilts are given in Fig.3(b). In the paraelectric phase the single mode experiences dramatic softening upon approaching the Curie point suggesting that this mode plays a critical role in the phase transition in agreement with the experimental findings of Ref.3. Below the Curie point the modes that are associated with the oxygen octahedra tilts about the antipolar axis of the AFE $PbZrO_3$ show softening, while the other modes appear to be rather insensitive to the temperature. Note, that softening of the modes associated with AFD motion were also observed experimentally[3]. Now let's turn to the temperature evolution of the Σ_2 modes above the Curie point given in Fig.3(c). The lowest frequency mode softens nearly to zero on approaching the phase transition, while other modes do not respond to the temperature. This demonstrates that the AFE mode associated with the vibrations of the lead ions also plays a critical role in the phase transition, nearly comparable to the role of the AFD mode. Note that these two modes do not share frequencies in the entire temperature range suggesting that they contribute to the phase transition rather independently. Thus, our computational findings provide the first evidence for the elusive AFE mode softening predicted by G.A. Samara in 1970[10]. Below the Curie point it appears that the highest frequency mode is the continuation of the highest frequency mode of the paraelectric phase. The lowest frequency mode is associated with the vibrations along the antipolar axis of AFE $PbZrO_3$ and shows considerable softening. Interestingly, the two lowest frequency modes at Σ_2 point share temperature evolution with the two lowest frequency AFD modes which sug-

gests that these modes are coupled. Similarly, the black and red branches in 150-180 cm^{-1} range share temperature evolution, once again indicating coupled motion. Finally, the last branch shared between AFE and AFD appear around 250 cm^{-1}. Note, that mode softening found in computations agree well with experimental data (see Fig.3(a)-(b)).

Our computational data suggest that, in agreement with experimental findings[3], the phase transition in $PbZrO_3$ is associated with softening of at least two lattice modes: one originating from the oxygen octahedra tilts and the other one associated with the lead ion vibrations. Moreover, the lead ion vibrations mode exhibits softening at both Γ and Σ_2 points of the PBZ consistent with the recent proposal that in $PbZrO_3$ the whole polarization branch is soft[3]. At the same time, we find that the softening of the polarization mode at the Γ point is somewhat moderate in comparison with other points investigated and in computations leads to only moderate increase in the static dielectric constant at the phase transition. The latter finding is, however, inconsistent with experimental findings which indicate a dielectric anomaly[7]. One possible explanation for the discrepancy could be that the zone center mode has mixed phonon and relaxational character. Our simulations capture phonon contribution but are likely to miss the relaxational one owing to the short simulation time and finite supercell size. Indeed, the experimental study on $PbZrO_3$ ceramics[11] reported only a slight softening of the polar mode with the associated contribution to the static dielectric constant of about 300 which are consistent with our findings (see Fig.3(a) and its inset). In that study the strong dielectric anomaly at the Curie point was attributed to the central mode rather than a soft displacive mode. Similarly, in the recent experimental study[2] the presence of the central peak was connected to the relaxational mode that shows critical softening at Γ point. Another possible reason for the discrepancy in the static dielectic constant between computations and experiments could be the overestimation of the energy difference between the FE and AFE phases of $PbZrO_3$ in computations. This, in turn, could be due to the defect free nature of the simulated sample. In real samples defects and impurities are unavoidable and some of them are known to stabilize the FE phase[18]. Another reason could be of methodological nature since we omit some of the degrees of freedom and retain only the most important interactions. Finally, we recall the earlier controversy regarding the structure of $PbZrO_3$. While first principles simulations (including the ones used for the parametrization of our effective Hamiltonian[8]) suggest nonpolar *Pbam* structure some of the earlier experimental data were consistent with the polar *Pba*2 structure that admits a zone

center polar mode[7]. In such samples we expect the FE phase to be even closer in energy to the AFE one.

IV. CONCLUSIONS

In summary, we have developed a computational approach that allows to compute mode dynamics at an arbitrary point of the Brillouin zone at finite temperatures. The power of such an approach is that it allows one to "see" the modes that are nearly invisible in experiments and, therefore, provide an in-depth insight into the dynamics of materials, including their phase transition. Application of this methodology to the prototypical AFE $PbZrO_3$ reveals the existence of multiple soft modes in this material both below and above the Curie point. Two modes are primarily responsible for the phase transition in $PbZrO_3$: one associated with the oxygen octahedra dynamics, while the other is due to lead ions dynamics. Within our model the entire branch of the lead ion modes appears to be soft with the minimum at the Σ_2 point of the PBZ. Our work provides the first computational insight into the dynamics of the phase transition in $PbZrO_3$ which complements the recent experimental efforts[2,3], and proposes a computational tool to study such dynamics in a class of similar materials for which experimental investigations are challenging.

ACKNOWLEDGMENTS

We thank J. Hlinka for useful discussions. The present work is supported by the U.S. Department of Energy, Office of Basic Energy Sciences, Division of Materials Sciences and Engineering under grant DE-SC0005245. Computer time was provided by USF Research Computing, sponsored in part by NSF MRI CHE-1531590.

---

[1] K. M. Rabe, "Antiferroelectricity in oxides: A reexamination," in *Functional Metal Oxides* (Wiley-VCH Verlag GmbH and Co. KGaA, 2013) p. 221.

[2] A. K. Tagantsev, K. Vaideeswaran, S. B. Vakhrushev, A. V. Filimonov, R. G. Burkovsky, A. Shaganov, D. Andronikova, A. I. Rudskoy, A. Q. R. Baron, H. Uchiyama, D. Chernyshov,

A. Bosak, Z. Ujma, K. Roleder, A. Majchrowski, J.-H. Ko, and N. Setter, Nat. Commun. **4** (2013).

[3] J. Hlinka, T. Ostapchuk, E. Buixaderas, C. Kadlec, P. Kuzel, I. Gregora, J. Kroupa, M. Savinov, A. Klic, J. Drahokoupil, I. Etxebarria, and J. Dec, Phys. Rev. Lett. **112**, 197601 (2014).

[4] R. W. Whatmore and A. M. Glazer, J. Phys. C: Solid State Phys. **12**, 1505 (1979).

[5] E. Sawaguchi, J. Phys. Soc. Jpn. **7**, 110 (1952).

[6] C. Kittel, Phys. Rev. **82**, 729 (1951).

[7] M. Lines and A. Glass, *Principles and Applications of Ferroelectrics and Related Materials* (Oxford, 2009).

[8] B. K. Mani, S. Lisenkov, and I. Ponomareva, Phys. Rev. B **91**, 134112 (2015).

[9] W. Cochran and A. Zia, phys. stat. sol. (b) **25**, 273 (1968).

[10] G. A. Samara, Phys. Rev. B **1**, 3777 (1970).

[11] T. Ostapchuk, J. Petzelt, V. Zelezny, S. Kamba, V. Bovtun, V. Porokhonskyy, A. Pashkin, P. Kuzel, M. D. Glinchuk, I. P. Bykov, B. Gorshunov, and M. Dressel, J. Phys.: Cond. Matter **13**, 2677 (2001).

[12] R. G. Burkovsky, A. K. Tagantsev, K. Vaideeswaran, N. Setter, S. B. Vakhrushev, A. V. Filimonov, A. Shaganov, D. Andronikova, A. I. Rudskoy, A. Q. R. Baron, H. Uchiyama, D. Chernyshov, Z. Ujma, K. Roleder, A. Majchrowski, and J.-H. Ko, Phys. Rev. B **90**, 144301 (2014).

[13] J. Íñiguez, M. Stengel, S. Prosandeev, and L. Bellaiche, Phys. Rev. B **90**, 220103 (2014).

[14] D. C. Rapaport, *The Art of Molecular Dynamics Simulation*, 2nd ed. (Cambridge University Press, 2004).

[15] D. Frenkel and B. Smit, *Understanding Molecular Simulations: From Algorithms to Applications* (Academic Press, 2010).

[16] C.-M. Chang, B. K. Mani, S. Lisenkov, and I. Ponomareva, Ferroelectrics **494**, 68 (2016).

[17] I. Ponomareva, L. Bellaiche, T. Ostapchuk, J. Hlinka, and J. Petzelt, Phys. Rev. B **77**, 012102 (2008).

[18] V. J. Tennery, J. Electrochem. Soc. **112**, 1117 (1965).

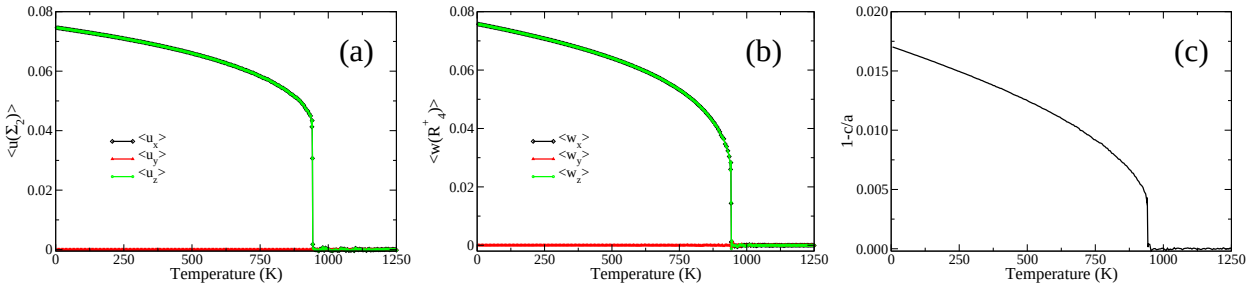

FIG. 1. (color online) Temperature evolution of the AFE (a) and AFD (b) order parameters (in units of the cubic lattice constant of $PbZrO_3$) and $1 - c/a$ ratio (c) from MD computations.

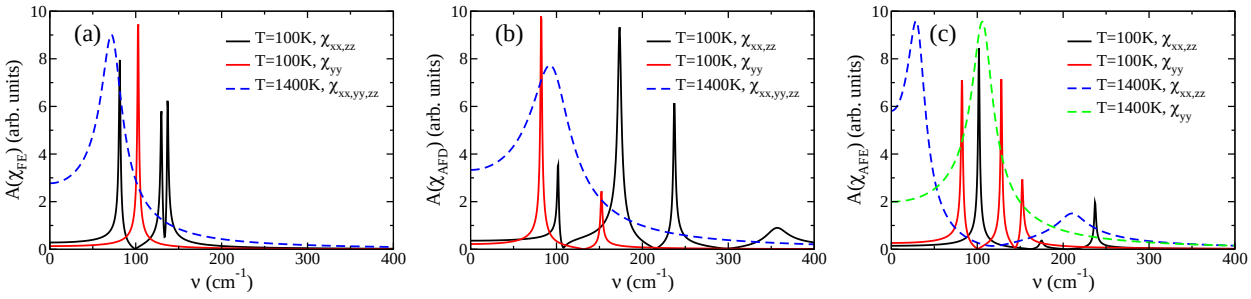

FIG. 2. (color online) Amplitudes for the components of the complex susceptibility tensors χ_{FE} (a), χ_{AFD} (b) and χ_{AFE} (c) for representative temperatures above (1400 K) and below (100 K) the Curie point. In the AFE phase the xx and yy components of the tensor are associated with the oscillations of the local modes along the antipolar direction, while yy component of the tensor originates from the oscillations along the nonpolar direction.

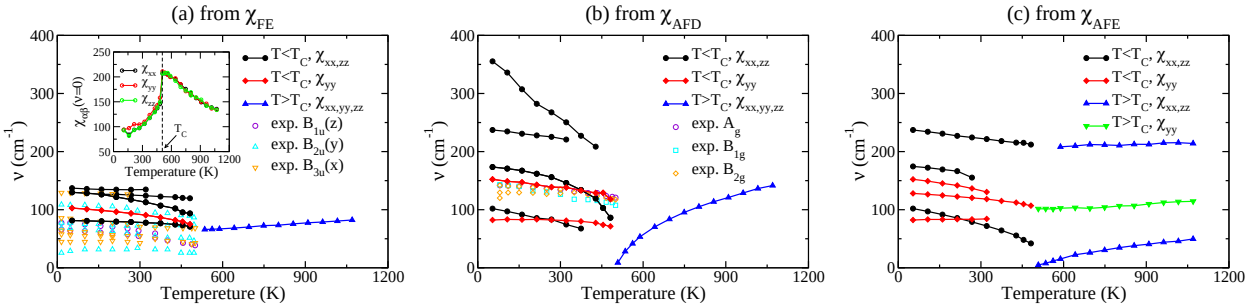

FIG. 3. (color online) Temperature evolution of the intrinsic modes frequencies as obtained from the fitting of generalized complex susceptibilities χ_{FE} (a), χ_{AFD} (b) and χ_{AFE} (c) [solid symbols]. Open symbols give experimental data from Ref.3. To facilitate comparison between computations and experiment computational temperatures were rescaled to reproduce experimental Curie point. In the AFE phase the xx and yy components of the tensor are associated with the oscillations of the local modes along the antipolar direction, while the yy component of the tensor originates from the oscillations along the nonpolar direction. In the paraelectric phase $\mathbf{q}_{\Sigma_2} = \frac{2\pi}{a}(1/4, 0, -1/4)$. The inset to Fig.3(a) gives the components of static susceptibility tensor obtained in computations. T_C indicates the Curie temperature.